Cancer Immunology, Immunotherapy (2025) 74:6
https://doi.org/10.1007/s00262-024-03860-w

RESEARCH

Three-dimensional dynamics of mesothelin-targeted CAR.CIK lymphocytes against ovarian cancer peritoneal carcinomatosis

Federica Galvagno[1,2] · Valeria Leuci[1,2] · Annamaria Massa[1,2] · Chiara Donini[1] · Ramona Rotolo[1] · Sonia Capellero[2] · Alessia Proment[1] · Letizia Vitali[1] · Andrea Maria Lombardi[1] · Valentina Tuninetti[1,3] · Lorenzo D'Ambrosio[1,4] · Alessandra Merlini[1,4] · Elisa Vigna[1] · Giorgio Valabrega[1,3] · Luca Primo[1,2] · Alberto Puliafito[1,2] · Dario Sangiolo[1]

Received: 6 September 2024 / Accepted: 9 October 2024

Abstract

Intraperitoneal cellular immunotherapy with CAR-redirected lymphocytes is an intriguing approach to target peritoneal carcinomatosis (PC) from ovarian cancer (OC), which is currently evaluated in clinical trials. PC displays a composite structure with floating tumor cells within ascites and solid-like masses invading the peritoneum. Therefore, a comprehensive experimental model is crucial to optimize CAR-cell therapies in such a peculiar environment. Here, we explored the activity of cytokine-induced killer lymphocytes (CIK), redirected by CAR against mesothelin (MSLN-CAR.CIK), within reductionistic 3D models resembling the structural complexity of both liquid and solid components of PC. MSLN-CAR.CIK effectively killed and were functionally efficient against OC targets. In a "floating-like" 3D context with floating OC spheroids, both tumor localization and killing by MSLN-CAR.CIK were significantly boosted by fluid flow. In a "solid-like" context, MSLN-CAR.CIK were recruited through the extracellular matrix on embedded tumor aggregates, with variable kinetics depending on the effector-target distance. Furthermore, MSLN-CAR.CIK penetrated the inner levels of OC spheroids exerting effective tumor killing. Our findings provide currently unknown therapeutically relevant information on intraperitoneal approaches with CAR.CIK, supporting further developments and improvements for clinical studies in the context of locoregional cell therapy approaches for patients with PC from OC.

Keywords 3D models · Cellular immunotherapy · Chimeric antigen receptor · Ovarian cancer · Peritoneal carcinomatosis

Introduction

Peritoneal carcinomatosis (PC) from ovarian cancer (OC) is a serious clinical condition, frequently associated with advanced stages and recurrent disease settings [1–3], where incomplete responses and relapses are still a major problem and the prognosis remains unsatisfactory, with a 5-year overall survival barely reaching 50% [4–6]. Advances in therapeutic approaches employed over the past two decades include surgery [7], first-line chemotherapy [8] and PARP inhibitors [9, 10], all determinants of significant clinical benefits, while, so far, immune checkpoint inhibitors have failed to demonstrate significant activity [11].

PC from OC is characterized by the spreading of tumor cells within the peritoneal cavity, adhering to the visceral and parietal peritoneum or floating in the accumulating peritoneal fluid defined as malignant ascites [1, 12]. The peculiar context of PC pathophysiology is well suited for locoregional administration of drugs which represent an active research frontier for this type of cancer [4, 13]. An intriguing perspective in this context is represented by the locoregional translation of cellular immunotherapies, where clinical trials are currently ongoing or just ended [14–17].

Alberto Puliafito and Dario Sangiolo have contributed equally to this article.

✉ Alberto Puliafito
alberto.puliafito@unito.it

✉ Dario Sangiolo
dario.sangiolo@unito.it

1 Department of Oncology, University of Torino, Turin, Italy

2 Candiolo Cancer Institute, FPO-IRCCS, Candiolo, TO, Italy

3 Medical Oncology, Ordine Mauriziano Hospital, Turin, Italy

4 Medical Oncology, AOU San Luigi Gonzaga, Orbassano, TO, Italy

Published online: 02 November 2024

Chimeric antigen receptor (CAR)-redirected cell-based immunotherapies are emerging as valuable opportunities and intense research efforts are currently devoted to translating the success obtained in hematological malignancies to solid tumors [18–21]. However, the ability of CAR.T cells to reach and infiltrate the solid tumor structure, which is critical for tumor eradication [22], is yet to be determined. In this regard, the case of PC is therefore a paradigmatic biological and clinical situation, because solid-like and liquid-like tumor components are both present. Therefore, assessing the efficacy of cell-based immunotherapy in PC from OC models might give important insights into the determinants of the efficacy of this particular therapeutic approach.

Here, we explored the activity of CAR-redirected cytokine-induced killer lymphocytes (CAR.CIK) against advanced OC, by developing suitable 3D models resembling the complexity of peritoneal metastasis. CIK are patient-derived ex vivo expanded lymphocytes [23], presenting a mixed T-NK phenotype and intrinsically endowed with HLA-independent antitumor activity consequent to the interaction of their main killing receptor (NKG2D) with stress-inducible targets (MIC A/B and ULBPs 1–6), commonly expressed by tumor cells [24]. The application of CIK as functional immune actors for CAR-cell therapy could bring improvements where conventional CAR.T cells present a poor therapeutic efficacy [25]. Furthermore, the choice of CAR.CIK with respect to CAR.NK or CAR.NKT lies in the ease of expansion ex vivo, a potentially longer persistence in vivo and higher efficacy against solid tumors [26]. CIK intrinsic NKG2D-mediated antitumor activity comes in help against challenging solid tumor settings characterized by the heterogeneous expression of the targeted antigen [19, 25, 27], thanks to the conjugation with CAR-specific targeting, as reported in different tumor types, including OC [25, 28–33]. In the peculiar context of OC, a hypothetical possibility is that of a regional intraperitoneal infusion of CAR.CIK, which provides the opportunity to focalize the antitumor activity and minimize the risk for systemic toxicities.

Here, we chose the well-described glycoprotein mesothelin (MSLN) as a CAR target for CAR-redirected CIK (MSLN-CAR.CIK) [34–37].

In order to dissect how the peculiar organization of PC may affect cell-based immunotherapy, we have developed reductionistic 3D models of both the solid and the floating components of PC. The intent is to shed light on the behavior of MSLN-CAR.CIK in the mixed context of PC from advanced OC, where locoregional therapeutic approaches are of current interest and thus further supporting the clinical studies that aim at exploring and optimizing the intraperitoneal delivery of a cell-based immunotherapy with CAR.CIK.

Materials and methods

Metastatic OC (mOC) cell lines

mOC cell lines, such as OVCAR-3 and OVCAR-4, were purchased from National Cancer Institute (NCI), OAW28, COV362, OAW42 from the European Collection of Authenticated Cell Cultures (ECACC) while SK-OV-3, and the control cell lines Caco-2, HeLa, and MRC-5 from American Type Culture Collection (ATCC). Except Caco-2, obtained from an established collection of CRC cell lines [38], all cell lines were kept in stock in our institute's cell culture facility, which reauthenticates cells by applying the PowerPlex16 Cell-ID assay (#DC6531, Promega, USA) and tests for *Mycoplasma* contamination with a PCR *Mycoplasma* Detection kit (#G238, Applied Biological Materials Inc., Canada). All cell lines have been characterized by the provider and maintained as suggested (see Supplementary Methods).

Generation and ex vivo expansion of MSLN-CAR.CIK

CIK were generated from peripheral blood mononuclear cells (PBMC) of patients with advanced stage tumors, including but not limited to OC, at Candiolo Cancer Institute and San Luigi Hospital, after releasing written informed consent according to internal Institutional Review Board (IRB)-approved protocols (no. 225/2015; no. 125/2022).

PBMC were isolated by density gradient centrifugation (#07851, Lymphosep, Aurogene, Roma, Italy) and seeded in cell culture flasks at a concentration of 2×10^6 cells/mL in RPMI-1640 medium (#ECB9006L, Euroclone S.p.A., Milano, Italy), consisting of 10% fetal bovine serum (#A5256701, Gibco BRL, ThermoFisher, Waltham, MA, USA), 100 U/mL penicillin and 100 µg /mL streptomycin (#ECB3001D, Euroclone S.p.A., Milano, Italy) and 2 mM L-glutamine (#ECB3000D-20, Euroclone S.p.A., Milano, Italy). We added IFN-γ (#130–096-482, Miltenyi Biotec, Bergisch Gladbach, Germany; 1,000 U/mL) on day 0 and after 24 h we activated PBMC using anti-Biotin MACSiBead Particles loaded with CD2, CD3, and CD28 antibodies (#130–091-441, Miltenyi Biotec, Bergisch Gladbach, Germany) and human interleukin (IL)-2 IS (#130–097-746, Miltenyi Biotec, Bergisch Gladbach, Germany, 300 U/mL). On day + 3, stimulated PBMC were transduced with third-generation bidirectional lentiviral vector [39] encoding for second-generation anti-MSLN-CAR containing 4-1BB co-stimulatory domain (Creative Biolabs Inc., Ramsey Road Shirley, NY, USA) and GFP reporter gene, by overnight incubation. Paired NTD.CIK were used as control. For selected experiments, activated PBMC were transduced with an irrelevant dNGFR/GFP-bidirectional lentiviral vector. Cells were expanded over 4 weeks. Fresh medium and IL-2

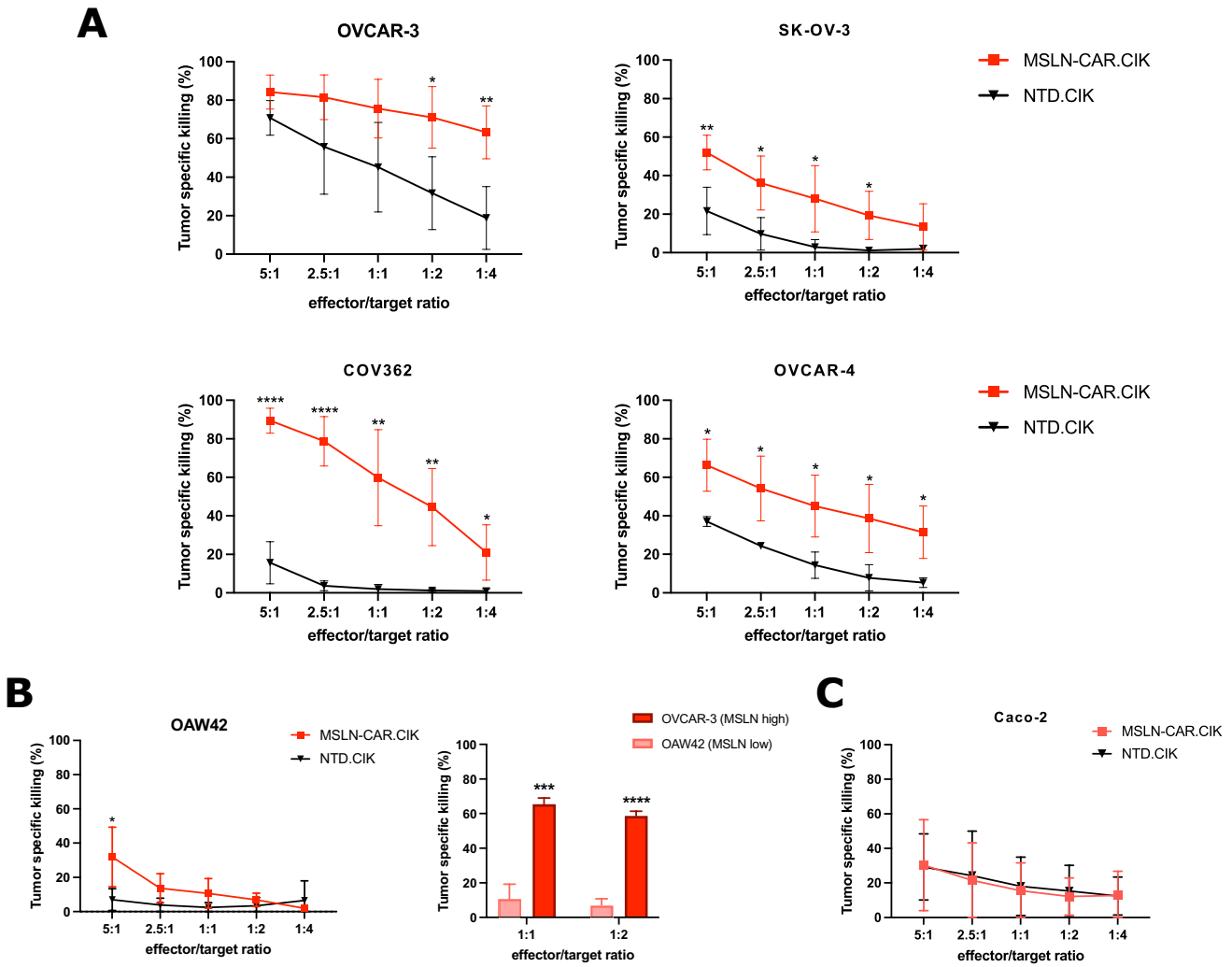

Fig. 1 MSLN-CAR.CIK effectively and specifically kill mOC cells in 2D. **A** MSLN-CAR.CIK killed mOC cell lines more specifically than NTD.CIK. Tumor cell-specific cytotoxicity values from > 3 biological replicates are reported (mean ± SD). **B** MSLN-CAR.CIK and NTD.CIK similarly killed the MSLN low mOC cell line OAW42 ($n = 4$) (mean ± SD) (left). MSLN-CAR.CIK killing of mOC cells depends on MSLN expression levels at therapeutically relevant E/T ratios ($n = 3/4$) (mean ± SD) (OVCAR-3 chosen as MSLN high cell line, while OAW42 as MSLN low) (right). **C** MSLN-CAR.CIK and NTD.CIK showed similar cytotoxic activity against colorectal cancer cell line Caco-2 not expressing MSLN ($n = 3$) (mean ± SD). (*$P \leq 0.05$; **$P \leq 0.01$; ***$P \leq 0.001$; ****$P \leq 0.0001$)

(300 U/mL) were replaced every 2–3 days as needed and the cell concentration was maintained at 1.8 × 10^6 cells/mL.

Tumor and MSLN-CAR.CIK characterization by flow cytometry

Conjugated CD3 (#552127), PD-1 (#565935) (BD Pharmingen, USA), and CD314 (anti-NKG2D) (#130–111-846), CD8 (#130–110-679), CD56 (#130–113-310) (Miltenyi Biotec, Germany) monoclonal antibodies (mAbs) were used to characterize phenotype of MSLN-CAR.CIK, and a conjugated anti-F(ab′)$_2$ fragment Ab (#115–606-072, Jackson ImmunoResearch Europe Ltd) to detect CAR expression. mOC cells were stained with conjugated mAbs for the expression of MIC A/B (#558352, BD Pharmingen, USA) and ULBPs-2,5,6 (#FAB1298A, R&D Systems Inc., USA). mOC was stained with 1 µg/mL MSLN-Ab (#PA5-79697, Sigma-Aldrich, USA), then washed and incubated with anti-rabbit IgG-AlexaFluor 647 Secondary Ab (#A31573, Invitrogen, ThermoFisher, USA).

Labeled cells were read on FACS Cyan ADP (Beckman Coulter, USA), analyzed using Summit Software (Beckman Coulter, USA), and on BDFACS Celesta (BD Life Sciences, USA). Gate criteria were set to secondary ab/unstained controls.

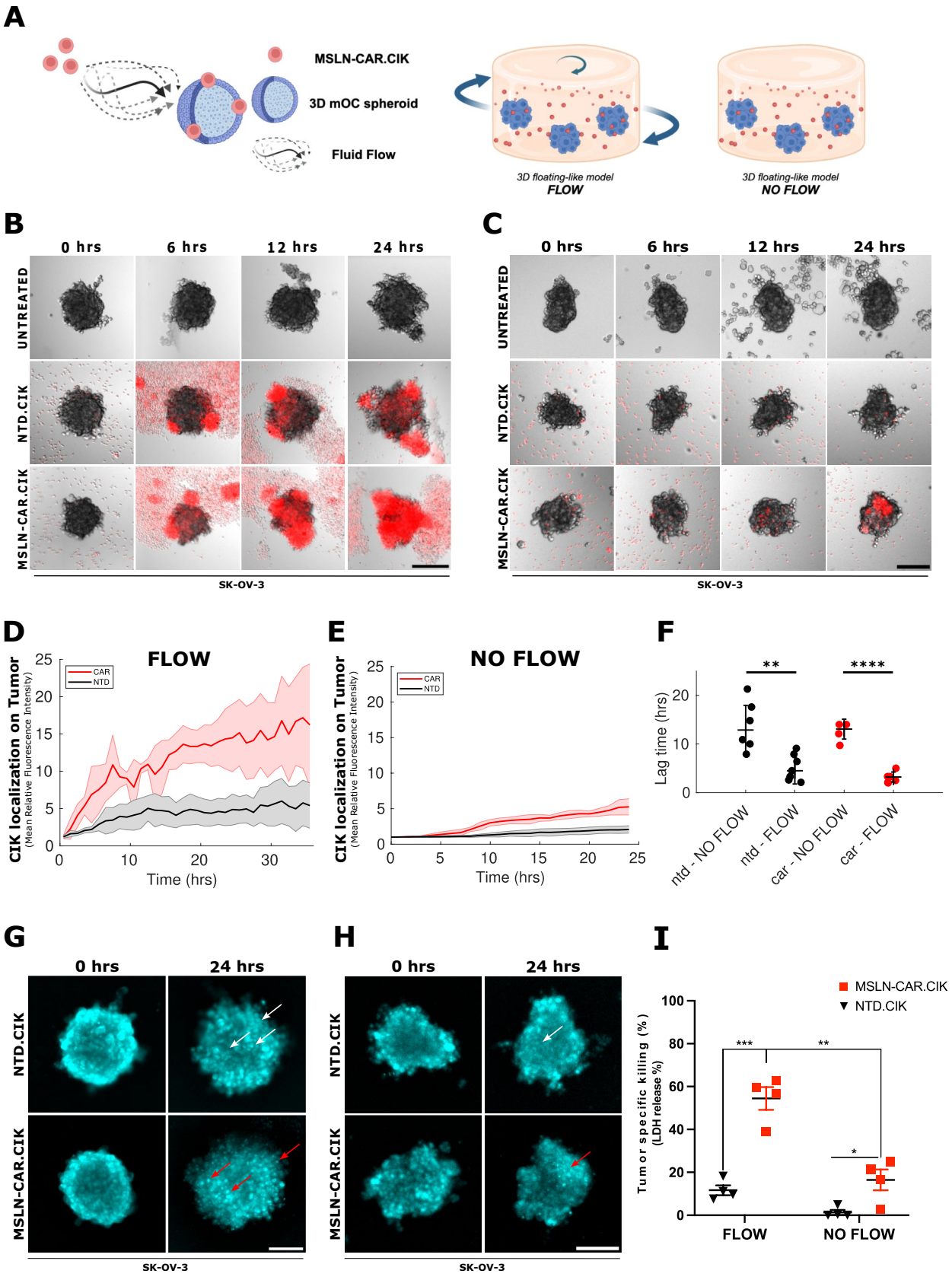
A
MSLN-CAR.CIK
3D mOC spheroid
Fluid Flow
3D floating-like model
FLOW
3D floating-like model
NO FLOW
B
0 hrs
6 hrs
12 hrs
24 hrs
UNTREATED
NTD.CIK
MSLN-CAR.CIK
SK-OV-3
C
0 hrs
6 hrs
12 hrs
24 hrs
UNTREATED
NTD.CIK
MSLN-CAR.CIK
SK-OV-3
D
FLOW
CAR
NTD
CIK localization on Tumor
(Mean Relative Fluorescence Intensity)
Time (hrs)
E
NO FLOW
CAR
NTD
CIK localization on Tumor
(Mean Relative Fluorescence Intensity)
Time (hrs)
F
**
****
Lag time (hrs)
ntd - NO FLOW
ntd - FLOW
car - NO FLOW
car - FLOW
G
0 hrs
24 hrs
NTD.CIK
MSLN-CAR.CIK
SK-OV-3
H
0 hrs
24 hrs
NTD.CIK
MSLN-CAR.CIK
SK-OV-3
I
MSLN-CAR.CIK
NTD.CIK
***
**
*
Tumor specific killing (%)
(LDH release %)
FLOW
NO FLOW

◂**Fig. 2** MSLN-CAR.CIK are more stably localized on the target when coupled with fluid flow in floating-like cultures. **A** Sketch of the reductionistic experimental floating 3D context (Created in BioRender.com). **B-C** MSLN-CAR.CIK cells were monitored by time-lapse imaging with (**B**) and without (**C**) flow, compared to NTD.CIK. Representative time-lapse microscopy images refer to snapshots at indicated timepoints for brightfield and fluorescence, the latter corresponding to lymphocytes only. Scale bar: 200 µm. **D**–**E** Measure of the intensity of fluorescence signal in the regions of the image corresponding to the spheroids. The plot shows the localization of lymphocytes on mOC spheroids in the presence (**D**) or absence (**E**) of a fluid flow at different times after the addition of MSLN-CAR.CIK. Each line represents the mean of many single spheroids (CAR flow $N=3$; NTD flow $N=3$; CAR no flow $N=5$; NTD no flow $N=3$), while shades represent SD. **F** Quantitative analysis obtained from localization data: localization time extracted by fitting the localization time sequences as fluorescent signal localized onto the tumor spheroids for MSLN-CAR.CIK vs NTD.CIK in the presence or absence of a flow. In floating cultures, mean and dispersions were (3.20 ± 1.02) h for MSLN-CAR.CIK ($N=5$ spheroids), compared with NTD.CIK (4.50 ± 2.72) h ($N=7$ spheroids). Localization time in static cultures had mean and dispersions of (13.05 ± 2.04) h for MSLN-CAR.CIK ($N=4$ spheroids), (12.85 ± 5.09) h for NTD.CIK ($N=6$ spheroids). **G**–**H** Representative images of mOC spheroids labeled with NucBlue and cultured with lymphocytes in the presence (**G**) or absence (**H**) of flow. Red arrows indicate small and fragmented nuclei, while white arrows indicate intact nuclei. Scale bar: 200 µm. **I** MSLN-CAR.CIK target more effectively 3D mOC spheroid in the presence of forced flow. LDH release from spheroids cultured in the presence or absence of fluid flow (n = 4) (mean ± SD). (*$P \leq 0.05$; **$P \leq 0.01$; ***$P \leq 0.001$; ****$P \leq 0.0001$)

Cancer cell spheroid formation

Three-dimensional (3D) mOC spheroids were generated from multiple mOC cell lines exploiting the hanging drop protocol [40], starting from preparation of a methylcellulose stock solution (see Supplementary Methods).

Spheroids premixed with Cultrex BME (#3434-050-RTU, R&D, Minneapolis, MN, USA) were seeded as described in the following paragraph. The number of cells per drop changed depending on the type of 3D assay. Generally, OVCAR-3: 200-750; SK-OV-3: 200-500-750; COV362: 200-750.

3D floating-like and solid-like models

We cultured 3D mOC aggregates employing two experimental settings: (I) to mimic floating metastasis, we set up a 3D floating-like model in which spheroids and MSLN-CAR.CIK were cultured in liquid medium, where the flow was enforced by mechanical shaking of the plate (using the BioTek Cytation3, Cell Imaging Multi-Mode Reader). (II) The 3D solid-like model was realized by embedding both spheroids and MSLN-CAR.CIK in a 3D hydrogel or seeding MSLN-CAR.CIK on top of the hydrogel.

(I) *3D floating-like models*

For the 3D floating-like cocultures, preassembled spheroids were cultured in 75 µL of culture media in ULA 96-well flat-bottomed plates (#6055802, PerklinElmer, USA) 3 days upon spheroids growing in hanging drop. The next day, MSLN-CAR.CIK were added in 75 µL of culture media with a final volume of 150 µL and IL-2 concentration of 300 U/mL. Differently from 2D assays, in the 3D case the effective number of effector to target cell ratios (E/T) was expressed in terms of volume densities rather than absolute numbers. The number of immune cells to be seeded in the culture medium was estimated by calculating the density of effector cells that could fit in a spherical shell (1000 µm radius) surrounding each tumor spheroid, in order to approximately generate a theoretical 1:1 E/T in the volume around all spheroids.

The cocultures were either maintained static or in the presence of a fluid flow for 24–36 h continuously or uncontinuously, to generate a fluid flow.

(II) *3D solid-like models*

For the 3D cell solid cultures, the preassembled spheroids were resuspended in a defined volume of Cultrex BME in order to reach c.a. a concentration of 10 spheroids every 45 µL of hydrogel per well, always maintaining the tube on ice.

In the 3D solid embedded culture, MSLN-CAR.CIK were premixed with the spheroids into the hydrogel at densities c.a. 2 × 10^6 cells/mL. Similar to the 3D floating-like models, the number of immune cells to be seeded in the gel was estimated by calculating the density of effector cells that could fit in a spherical shell (390–450 µm radius) surrounding each tumor spheroid, in order to approximately generate a theoretical 1:1 E/T around all spheroids. Forty-five µL of the embedded mixture supplemented with 300 U/mL of IL-2 was pipetted per well into a black-walled, glass-bottom, 96-well imaging plate (#0030741030, Eppendorf, Germany) and allowed to polymerize for 30 min in the incubator at 37 °C, 5% CO2. After polymerization, the scaffolds were covered with 150 µL of RPMI-1640 supplemented with 300 U/mL of IL-2.

In the 3D solid top culture, spheroids were embedded in 45 µL of Cultrex BME alone and covered with a volume of 150 µL of RPMI-1640 plus IL-2 (300 U/mL) with a given number of MSLN-CAR.CIK.

To evaluate immune effector infiltration, the 3D solid embedded culture was re-adapted to fit in a µ-slide 18-well chamber slide (#81816, IBIDI, Germany). MSLN-CAR.CIK were premixed with the spheroids into the hydrogel at densities c.a. 14 × 10^6 cells/mL. The number of immune cells to be seeded in the gel was estimated by calculating the density of effector cells that could fit in a spherical shell (150 µm radius) surrounding each tumor spheroid. Forty µL of the embedded mixture was pipetted per well and allowed to polymerize for 30 min in the incubator at 37 °C, 5% CO2. After

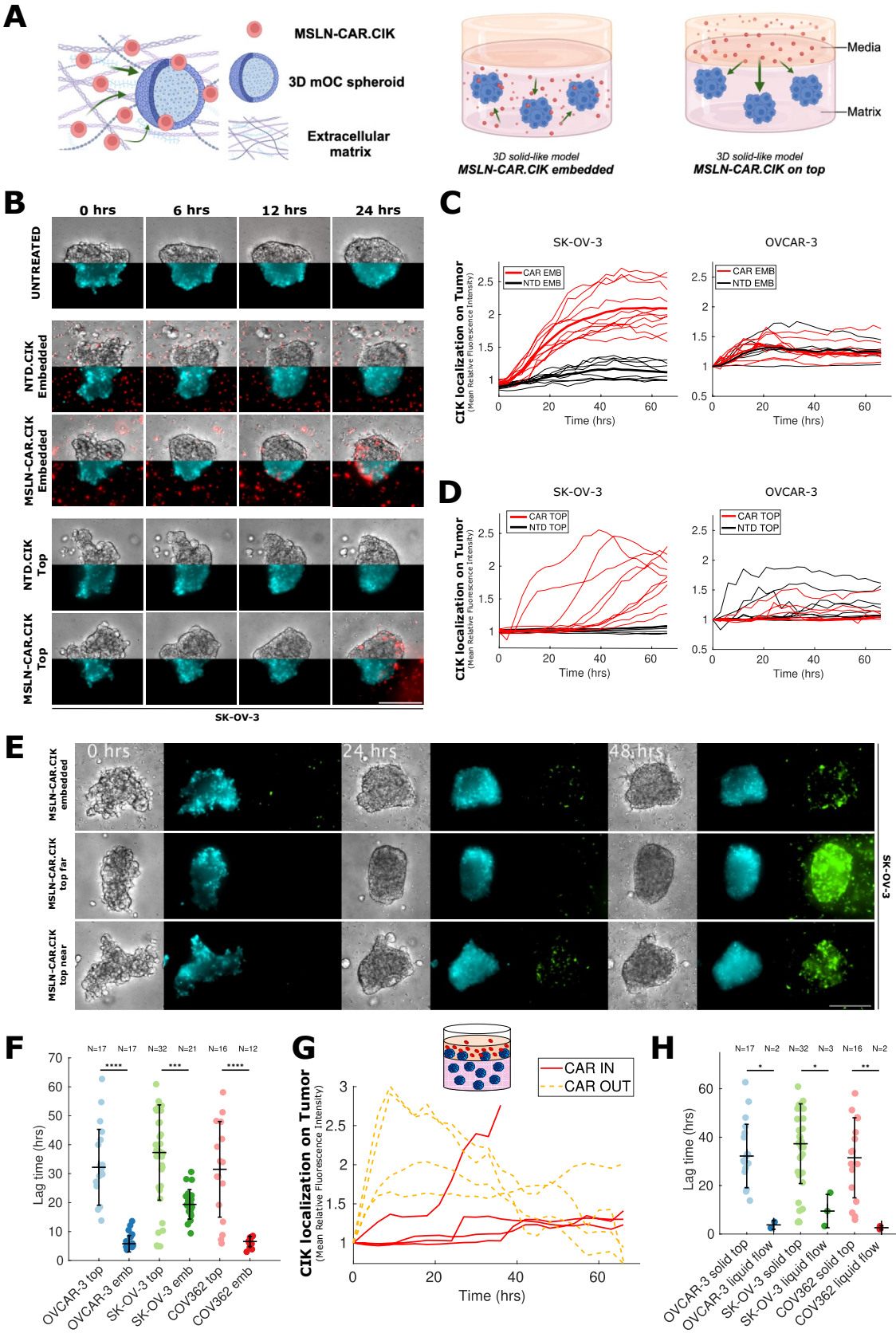
A
MSLN-CAR.CIK
3D mOC spheroid
Extracellular matrix
Media
Matrix
3D solid-like model
MSLN-CAR.CIK embedded
3D solid-like model
MSLN-CAR.CIK on top
B
0 hrs
6 hrs
12 hrs
24 hrs
UNTREATED
NTD.CIK Embedded
MSLN-CAR.CIK Embedded
NTD.CIK Top
MSLN-CAR.CIK Top
SK-OV-3
C
SK-OV-3
OVCAR-3
CAR EMB
NTD EMB
CIK localization on Tumor
(Mean Relative Fluorescence Intensity)
Time (hrs)
D
SK-OV-3
OVCAR-3
CAR TOP
NTD TOP
CIK localization on Tumor
(Mean Relative Fluorescence Intensity)
Time (hrs)
E
0 hrs
24 hrs
48 hrs
MSLN-CAR.CIK embedded
MSLN-CAR.CIK top far
MSLN-CAR.CIK top near
SK-OV-3
F
N=17 N=17 N=32 N=21 N=16 N=12
****
***
****
Lag time (hrs)
OVCAR-3 top
OVCAR-3 emb
SK-OV-3 top
SK-OV-3 emb
COV362 top
COV362 emb
G
CAR IN
CAR OUT
CIK localization on Tumor
(Mean Relative Fluorescence Intensity)
Time (hrs)
H
N=17 N=2 N=32 N=3 N=16 N=2
*
*
**
Lag time (hrs)
OVCAR-3 solid top
OVCAR-3 liquid flow
SK-OV-3 solid top
SK-OV-3 liquid flow
COV362 solid top
COV362 liquid flow

◂**Fig. 3** MSLN-CAR.CIK migrate and are recruited on mOC tumor spheroids. **A** Sketch of the reductionistic experimental solid 3D contexts (Created in BioRender.com). **B** MSLN-CAR.CIK and NTD.CIK were monitored by time-lapse imaging when embedded in the hydrogel (upper three rows) and when seeded on top (lower two rows) against mOC spheroids**.** Representative microscope images refer to snapshots at indicated times where the top half of the image is the brightfield channel while the lower part corresponds to tumors labeled with NucBlue, and for both the additional fluorescent channel corresponds to lymphocytes. Scale bar: 200 μm. **C**–**D** Intensity of fluorescence signal in the regions of the image corresponding to the spheroids. The plot shows the recruitment of MSLN-CAR.CIK or NTD.CIK on mOC spheroids when embedded **C** or seeded on top of the matrix (**D**), as a function of time. Each thin line represents a single spheroid, while the ticker lines represent the median. **E** Comparison of MSLN-CAR.CIK monitored by time-lapse imaging when embedded in the hydrogel with respect to when seeded on top of it, targeting mOC spheroids embedded at different distances from the liquid–matrix interface**.** mOC spheroids are labeled with NucBlue (cyan) and CAR lymphocytes labeled with PKH67 (green). Grayscale images correspond to brightfield images. Each row shows a mOC spheroid either co-embedded with MSLN-CAR.CIK (upper row) or alone (middle–lower rows), in representative snapshots at indicated times for each channel. Scale bar: 200 μm. **F** Lag time of recruitment on tumor spheroids for MSLN-CAR.CIK embedded or seeded on top of the hydrogel for each considered mOC cell line. For example, OVCAR-3 cell line challenged with MSLN-CAR.CIK, results in a lag time (31.50 ± 16.53) h when embedded ($N = 17$ spheroids), versus (6.55 ± 1.71) h when on top ($N = 17$ spheroids). **G** The plot shows the recruitment of MSLN-CAR.CIK when seeded on top of the hydrogel against mOC spheroids seeded both on top of as well (CAR OUT) or completely embedded in (CAR IN). **H** Recruitment time of MSLN-CAR.CIK when seeded on top of the hydrogel in a 3D solid-like model or in a 3D floating-like model under a forced fluid flow for each considered mOC cell line. For example, OVCAR-3 cell line challenged with MSLN-CAR.CIK, results in a lag time (31.50 ± 16.53) h when on top of the hydrogel ($N = 17$ spheroids), versus (2.60 ± 0.85) h in a forced flow ($N = 2$ spheroids). ($^{*}P \leq 0.05$; $^{**}P \leq 0.01$; $^{***}P \leq 0.001$; $^{****}P \leq 0.0001$)

polymerization, the scaffolds were covered with 100 μL of RPMI-1640 supplemented with 300 U/mL of IL-2.

3D floating-like tumor cell killing assays

In 3D floating-like models, mOC spheroids were seeded five per well in ULA 96-well flat bottom plates. MSLN-CAR.CIK and NTD.CIK were plated at a given volume density recapitulating a E/T of 1:1 in culture medium with 300 U/mL IL-2, 25 mM HEPES at 37 °C 5% CO2. Immune-mediated cytotoxicity against mOC spheroids was determined using CytoTox 96 Non-Radioactive Cytotoxicity Assay kit (#G1780, Promega, USA) upon 24 h of continuous mechanical shaking of the coculture (freq. 150 r.p.m.), as described in Supplementary Methods.

3D solid-like tumor cell killing assays

In 3D solid-like models, NucBlue (#R37605, Invitrogen, ThermoFisher, USA)-positive mOC spheroids and PKH67 (#P7333, Sigma-Aldrich, USA)-positive MSLN-CAR.CIK or NTD.CIK were cultured for 72 h, upon staining with propidium iodide (#P4170, Sigma-Aldrich, USA). Killing activity was determined as positivity of propidium iodide fluorescence spheroid area (pixel). Untreated mOC spheroids were used to evaluate spontaneous mortality, whereas a part was lysed with 5% *(v/v)* Triton X-100 (#1610407, Bio-Rad, Hercules, USA) as a control for the maximum cytotoxicity.

Imaging and quantitative image processing

Details on live imaging, cell labeling, and image quantification techniques are detailed in the **Supplementary Information**.

Statistical and data analysis

Data were analyzed using Prism 10.0 (GraphPad Software) or MATLAB (The Mathworks, USA). Descriptive data are presented as mean or median values, and all error bars represent standard deviation (SD). Statistical significance was obtained with two-tailed unpaired Student's t tests. A $P \leq 0.05$ was considered significant. Significance is represented as *, $P \leq 0.05$; **, $P \leq 0.01$; ***, $P \leq 0.001$; **** $P \leq 0.0001$.

Results

MSLN-CAR.CIK are functional in 3D biological models recapitulating the complexity of PC

MSLN-CAR.CIK were first generated and characterized and the relative cytotoxic activity was tested in standard two-dimensional killing assays on a panel of mOC cell lines (Supplementary Fig. S1). MSLN-CAR.CIK effectively killed tumor targets at all E/T ratios, with clear improvements compared to NTD.CIK (Fig. 1A and Supplementary Fig. S2A). As expected, MSLN-CAR.CIK-mediated tumor toxicity was strongly dependent on the level of surface expression of MSLN on tumor cells, as shown by comparing mOC cell lines negative or positive for MSLN (Fig. 1A-B and Supplementary Fig. S2B). MSLN-CAR.CIK and NTD.CIK showed instead comparable cytotoxicity against the MSLN-negative control Caco-2 cell line (Fig. 1C) and limited activity against non-tumoral fibroblast cell line MRC-5 (Supplementary Fig. S2C). A higher cytotoxic activity, retained even at lower E/T ratios, was observed by MSLN-CAR.CIK as compared with CIK engineered with the irrelevant dNGFR/GFP-bidirectional lentivirus (Supplementary Fig. S2D).

In order to recapitulate the clinical complexity of peritoneal metastasis and to be able to appreciate the dynamical interactions between MSLN-CAR.CIK and tumor cells, we

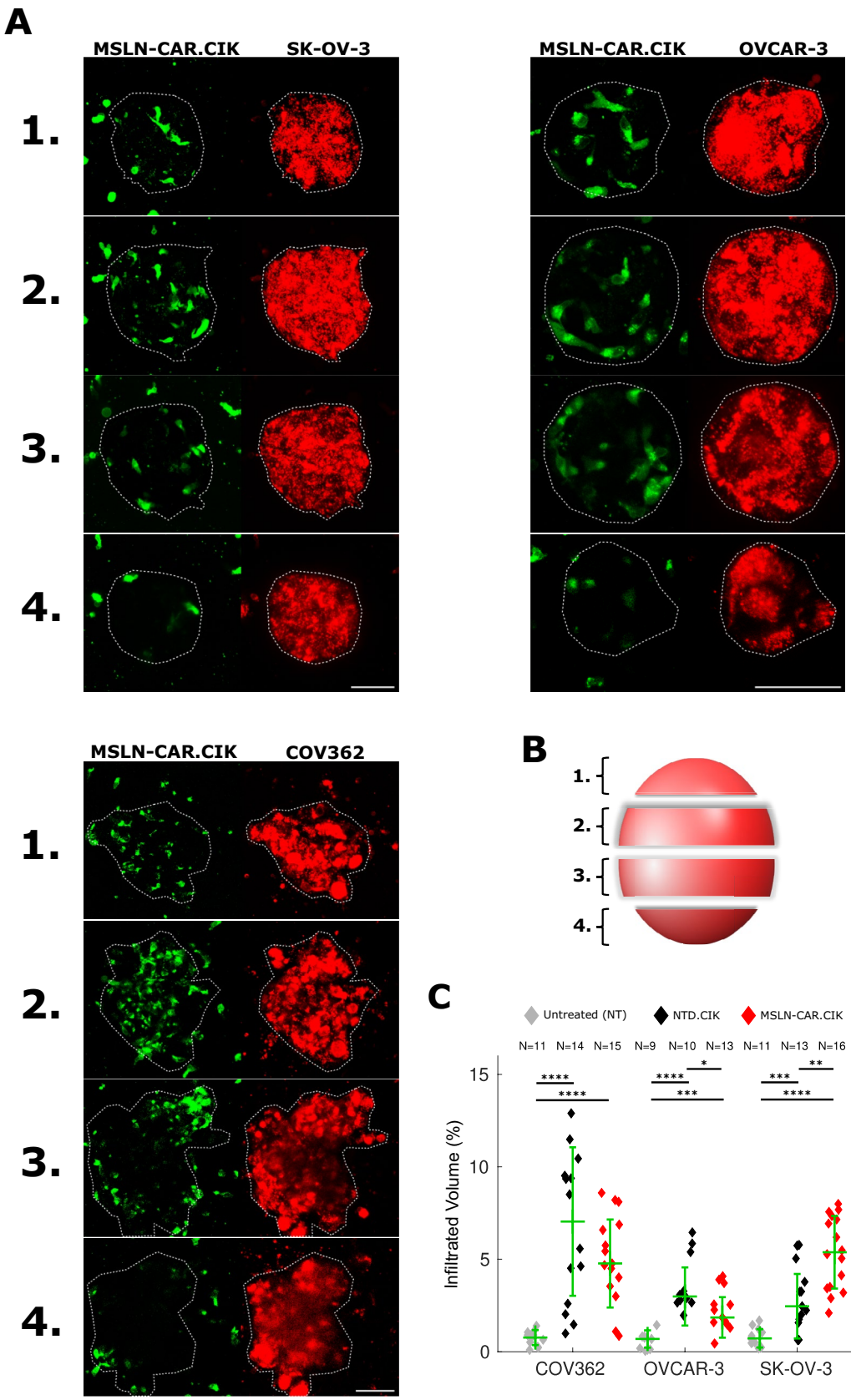
A
MSLN-CAR.CIK
SK-OV-3
MSLN-CAR.CIK
OVCAR-3
MSLN-CAR.CIK
COV362
1.
2.
3.
4.
B
1.
2.
3.
4.
C
Untreated (NT)
NTD.CIK
MSLN-CAR.CIK
N=11 N=14 N=15 N=9 N=10 N=13 N=11 N=13 N=16
Infiltrated Volume (%)
0
5
10
15
COV362
OVCAR-3
SK-OV-3

◂**Fig. 4** MSLN-CAR.CIK infiltrate the tumor target in a 3D solid-like biological setting. **A** Maximum intensity projections of four grouped confocal sections of mOC spheroids challenged with MSLN-CAR.CIK, both embedded in 3D hydrogel after 16 h of coculture. (MSLN-CAR.CIK: green—PKH67; mOC spheroid: red—PKH26). Scale bar: 50 µm. **B** Sketch of the mOC spheroid sectioning done to generate four different maximum intensity projections along the z-plane of each spheroid. **C** Fraction of mOC spheroid volume occupied by MSLN-CAR.CIK or NTD.CIK, obtained by quantifying the segmented signal within the spheroid volume. (*$P \leq 0.05$; **$P \leq 0.01$; ***$P \leq 0.001$; ****$P \leq 0.0001$)

developed reductionistic experimental settings for the solid-like and floating-like components of PC.

MSLN-CAR.CIK localize effectively on the floating component of mOC

To mimic the floating metastasis subjected to fluid flows potentially generated by body-movement, we cultured mOC spheroids and MSLN-CAR.CIK in liquid medium, where the fluid flow was enforced by mechanical shaking of the plates, as sketched in Fig. 2A and Supplementary Fig. S3A. In relative terms, MSLN-CAR.CIK localized more intensely on mOC spheroids than NTD.CIK, regardless of the presence of the flow. Importantly, MSLN-CAR.CIK localization on mOC spheroids was significantly faster and stronger in the presence of fluid flows than in its absence (Fig. 2B–E and Supplementary Video S1, S2). Localization of MSLN-CAR.CIK in the presence of a fluid flow took on average (3.2 ± 1.0) h, while it took (4.5 ± 2.7) h for control NTD.CIK (Fig. 2F). The absence of flow greatly increased the recruitment time, with an average of (13.1 ± 2.0) h for MSLN-CAR.CIK and (12.9 ± 5.1) h for NTD.CIK (Fig. 2F). Details on the measurement of the recruitment time can be found in Supplementary Methods.

MSLN-CAR.CIK are cytotoxic against the floating component of mOC

In the floating 3D context, we found that MSLN-CAR.CIK retained the intense cytotoxicity observed in the traditional 2D assay (Fig. 1A).

Qualitatively, the cytotoxic activity of MSLN-CAR.CIK in the presence of fluid flow is indicated by evident fragmentation of nuclei induced by the CAR lymphocytes, compared with images taken at the beginning of the coculture, as shown in Fig. 2G and H. In order to quantitatively corroborate this observation, we measured cytotoxicity by assessing the release of lactate dehydrogenase (LDH) in the culture medium. Our data indicate that MSLN-CAR.CIK were significantly more cytotoxic in the presence of a continuously forced fluid flow, coherently with the faster localization of CAR lymphocytes on the target (Fig. 2I). The relative enhanced cytotoxicity by MSLN-CAR.CIK vs NTD.CIK was also coherent with the stronger tumor localization of MSLN-CAR.CIK, thereby yielding a systematically higher killing independently of the fluid flow (Fig. 2I).

MSLN-CAR.CIK are recruited on the solid component of PC with kinetics dependent on target-effector distance

In order to assess whether MSLN-CAR.CIK can effectively reach and kill targets in the solid-like setting, we set up a hydrogel embedded 3D culture to mimic the extracellular matrix. CAR lymphocytes and tumor spheroids were cocultured in two different experimental conditions in which effectors were either added on the liquid–gel interface, recapitulating a more realistic setup to evaluate their ability to migrate from the liquid to the solid matrix, or embedded within the gel, recapitulating a more homogeneous and reproducible setup (Fig. 3A and Supplementary Fig. S3A). MSLN-CAR.CIK effectively localized on matrix-embedded tumor spheroids.

As expected, MSLN-CAR.CIK were recruited more rapidly when initially embedded in the matrix (Fig. 3B upper panels—C and Supplementary Video S3). MSLN-CAR.CIK also penetrated the hydrogel (Fig. 3B lower panels—D) from the liquid–matrix interface, albeit with more variable recruitment times, suggesting a potential dependence on the distance of the target from the interface. Coherently, when observed for longer times (72 h), similar levels of MSLN-CAR.CIK recruitments were reached, independently from where the immune cells were initially located (Fig. 3C–E and Supplementary Video S4). This observation was corroborated by the direct comparison of the distribution of lag-times in the two different settings (termed top and embedded, Fig. 3F), which highlights a much broader distribution for CAR lymphocytes seeded on top of the matrix than when embedded. The dependence of the time required to reach the mOC spheroids on the distance traveled by the CAR lymphocytes was confirmed by direct measurements of the location of mOC spheroids as shown in Supplementary Fig. S4A. To further test the specificity of MSLN-CAR.CIK, we measured their localization on 3D non-tumoral fibroblast aggregates and found it to be lower than on tumor cells (Supplementary Fig. S3B, C).

Since metastatic implants in patients can also be found adhered at the liquid–matrix interface, we performed experiments by seeding mOC spheroids both on top of the matrix as well as completely embedded as shown in Fig. 3G, and then added MSLN-CAR.CIK on the liquid–gel interface. Our results outlined how MSLN-CAR.CIK recruitment over superficial spheroids (CAR OUT) was almost

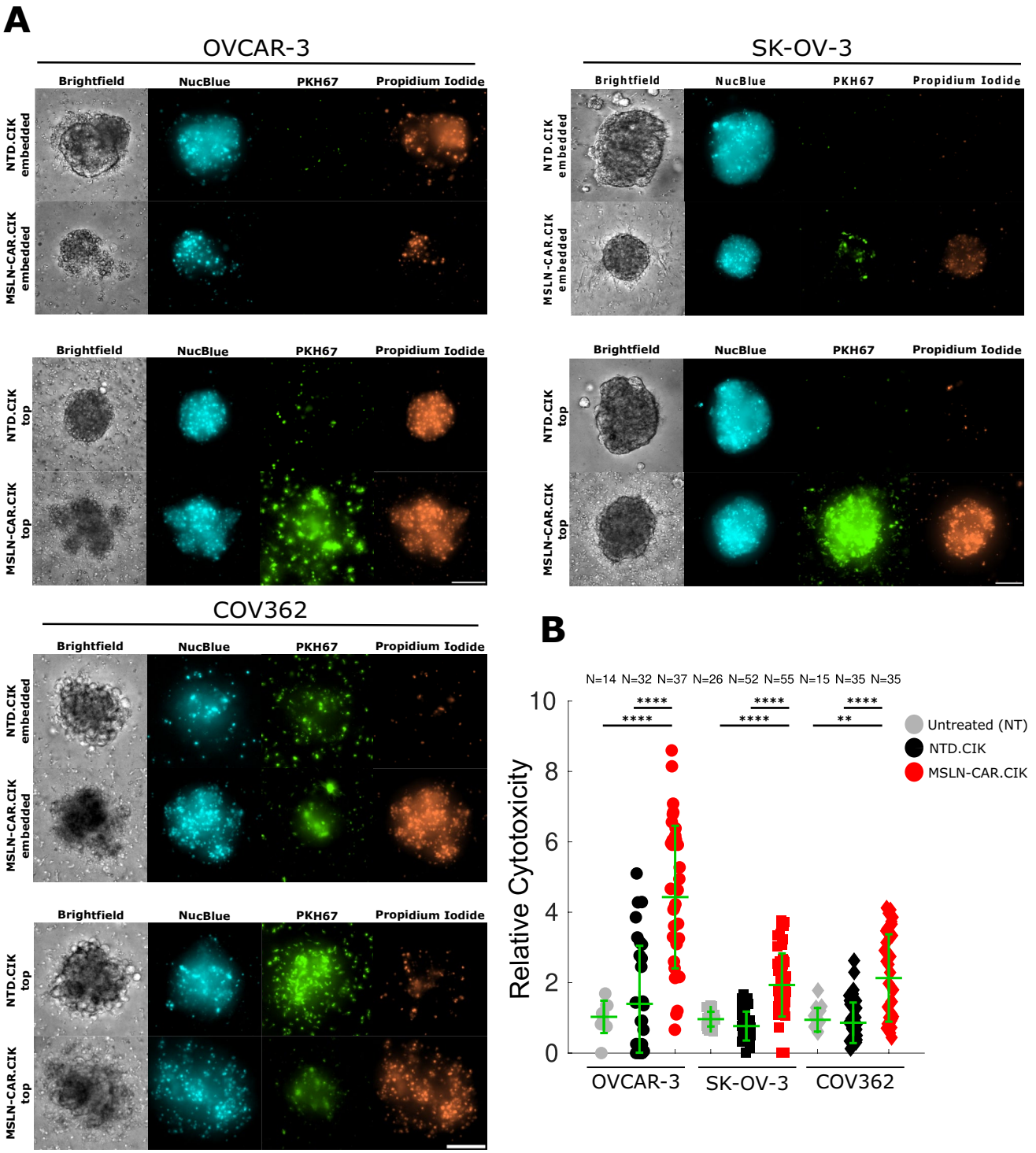

Fig. 5 MSLN-CAR.CIK are cytotoxic against the solid component of PC in 3D solid-like biological settings. **A** Comparison of MSLN-CAR.CIK- and NTD.CIK-treated mOC spheroids lapsed after 72 h of coculture, when CAR lymphocytes are embedded in the hydrogel with respect to when seeded on top of it. mOC spheroids are labeled with NucBlue (cyan), CIK with PKH67 (green), and the killing effect is shown by propidium iodide labeling (orange). Grayscale images correspond to brightfield images. Scale bar: 100 µm. **B** Cytotoxic activity on single mOC spheroids either untreated (gray), cocultured with MSLN-CAR.CIK (red) or with NTD.CIK (black) in both 3D solid-like models, all related to untreated condition. Green bars correspond to median and SD. (**$P \leq 0.01$; ****$P \leq 0.0001$)

immediate without, however, compromising the ability of the MSLN-CAR.CIK to target inner mOC spheroids (CAR IN) (Fig. 3G).

It is worth noting that the typical recruitment times obtained in experiments performed in the solid-like model are estimated around one order of magnitude larger than those obtained in the floating-like models (Fig. 3H), coherently with the quantitative argument presented in Supplementary Information S1.

MSLN-CAR.CIK infiltrate and kill the solid component of PC

As a final experimental validation of our cell therapy approach, we found that MSLN-CAR.CIK infiltrate deep layers of the tumor spheroids and exert a significant cytotoxicity.

By confocal microscopy we verified that, already after 16 h, mOC spheroids embedded in the matrix and cocultured with embedded lymphocytes are found clearly infiltrated with MSLN-CAR.CIK (Fig. 4A–C and Supplementary Fig. S4B). These findings support the notion that MSLN-CAR.CIK can reach and infiltrate in a 3D solid-like biological setting, which is a prerequisite for an efficient destruction of solid masses.

Finally, we investigated the MSLN-CAR.CIK cytotoxic activity against tumor targets in a solid-like environment (Fig. 5A), and verified that MSLN-CAR.CIK exert a significant cytotoxic effect, ranging from approximately two to fourfold higher than baseline level of spontaneous mortality of untreated tumor spheroids, peaking around fourfold for OVCAR-3, consistently with 2D killing assays (Fig. 5B—Supplementary Fig. S4C).

Taken together these data indicate that the killing ability of MSLN-CAR.CIK in 3D is systematically and significantly higher than that of NTD.CIK. This observation is coherent with our results on 2D killing assays which indicate MSLN-CAR.CIK as more cytotoxic than NTD.CIK.

Discussion

The central aim of our research was the development of a reductionistic and reliable experimental 3D setting that recalled independently the floating-like and solid-like components of PC, to model the spatio-temporal dynamics and antitumor activity of MSLN-CAR.CIK therapy. Our intent was to gain insights into specific variables that could be relevant and considerable in planning experimental trials of CAR.CIK locoregional treatments into the peritoneal cavity.

A relevant aspect of our model is the fluid flow mediated transport which is a peculiarity of the floating-like setting. A fluid flow is instead substantially absent in the solid-like setting, where cell transport is due to active cell migration through the extracellular matrix, and potentially significantly slower. Coherently, our data highlighted the positive contribution of a fluid flow on the kinetics of MSLN-CAR.CIK localization over targets with respect to the case where fluid flow is absent. In the setting of a clinical intraperitoneal infusion, these findings support the idea that MSLN-CAR.CIK might benefit from the liquid compartment dynamics of PC and that such a therapeutic approach may therefore require and be adapted to a correct movement schedule for the treated patients.

It is conceivable that the migration of MSLN-CAR.CIK within the matrix is sustained by a chemotactic gradient which drives and orient cell migration over the tumor target [41, 42]. In a forced fluid flow, concentration gradients might be destroyed partially or completely by fluid flow mixing, thereby reducing or eliminating the role of spatially oriented diffusible cues. Such differences between the two conditions might determine the diversity of timescales, which nonetheless allow MSLN-CAR.CIK to get in contact with and attack the different types of tumor lesions in both experimental settings. A direct clinical consequence would be a time delay in the destruction of the two types of lesions in mOC patients, with the floating ones being likely eliminated first.

The capacity of MSLN-CAR.CIK to infiltrate and destroy 3D mOC targets was clearly demonstrated in our model. In particular, our data indicate that infiltration is not only happening on the external surface of tumor spheroids but also deeper inside, endowing MSLN-CAR.CIK with an even higher killing potential due to favorable geometric aspects. Indeed, our data further support the strategies that are currently object of study both at the preclinical and clinical levels aimed at minimizing the target-to-tumor distance, thereby enhancing the chance of interactions between immune effectors and targets, like in the case of intraperitoneal infusions [14, 15, 43, 44]. On this side, our results also indicate that the floating component does not compromise the ability of the immune effectors to target inner, matrix-embedded, targets, supporting the notion that the coexistence of both liquid and solid PC compartments can be tackled by the same therapeutic approach, thus confirming the efficacy of locoregional administration of CAR-cell immunotherapy.

It is important to note that the experimental model of recruitment kinetics and 3D interactions described in our work can in principle apply to other cell therapies employing different immune effectors, as well as to other solid cancers, where cell immunotherapy approaches with regional infusions are being investigated [43, 45, 46].

Here, we propose MSLN-CAR-redirected CIK lymphocytes as functional immune effectors which present an HLA-independent and NKG2D-mediated killing activity, coupled with the CAR-specific activity [25, 33], as a functional

way to address and counteract the antigenic heterogeneity that CAR-cell therapies face and in addition to the antigen spreading elicited upon CAR-mediated tumor lysis [47, 48]. It is worth noting that the activation of MSLN-CAR.CIK by target engagement may prompt a favorable bystander effect against tumor cells with lower or negative MSLN expression, similarly to what reported for T cells [49, 50]. Our data support and validate MSLN as a suitable tumor target antigen for CAR-therapies against advanced OC, in line with previous evidence reported with CAR.T cells [51, 52]. The observed intense antitumor activity, maintained even at unfavorable E/T ratios, is encouraging and relevant for current ongoing and future clinical trials [16].

Overall, our work provides an integrated experimental platform, capable of exploring and monitoring the functionality of CAR.CIK against 3D tumor targets, taking into account elements of both the floating and solid components of PC. The model allows to expose, consider, and longitudinally measure independent variables, striving for a cell-resolved level of analysis, addressing current limitations of standard cell-based immunological assays and murine models.

Future work shall address additionally the adherence of our 3D models to the real PC pathophysiology. For instance, it is worth to verify the compatibility of CAR.CIK therapies to the altered ascites microenvironment [53] and possibly propose new strategies to optimize their efficacy [54, 55]. In the prospect of an adjuvant approach to standard chemotherapies, testing combinatorial treatment will be crucial.

In vivo experimental approaches based on murine models, in the context of disseminated OC and locoregional delivered CAR-cell therapy [51, 56], will be of paramount importance in order to confirm our findings, even though on a bulk-resolved level of inspection. A first important scientific question is whether locoregional administration has better pharmacokinetics and antitumor efficacy, not only in the cellular ascitic compartment but also in the solid compartment. Further, MSLN-CAR.CIK adoptive cell therapy can be challenged in the highly relevant context of minimal residual disease or platinum resistance, where this approach might firstly be explored in clinical studies. Lastly, the effect of fluid flow on the cell intraperitoneal infusion could be tested in animal models, by creating a dedicated movement schedule for mice and assessing the efficacy of therapy accordingly.

In a clinical perspective, our findings shed insights on the mechanisms of action of CAR.CIK against PC from advanced OC delivered as an intraperitoneal cellular immunotherapy, concurrent to the ongoing clinical studies, and pointing out the relevant difference in the timescales of tumor elimination that may be present.

Supplementary Information The online version contains supplementary material available at https://doi.org/10.1007/s00262-024-03860-w.

Acknowledgements The authors would like to thank Dr. Antonio Celani for fruitful discussion and Dr. Lara Fontani and Dr. Jessica Erriquez for experimental support.

Author contributions All authors read and approved the final version of the manuscript. Conceptualization was performed by F.G., V.L., E.V., L.P., A.P., and D.S.; Data curation was performed by F.G., V.L., A.M., C.D., R.R., A.Pr., L.V., and A.M.L.; investigation was done by F.G., V.L., A.M., C.D., R.R., S.C., A.Pr., L.V., and A.M.L.; methodology was performed by F.G., V.L., S.C., E.V., L.P., and A.P.; validation was performed by F.G.; formal analysis and visualization were conducted and optimized by F.G. and A.P.; writing—original draft was performed by F.G., A.P., and D.S.; writing—review and editing was revised by F.G., V.L., A.M., C.D., R.R., S.C., A.Pr., L.V., A.M.L., V.T., L.D., A.Me., E.V., G.V., L.P., A.P., and D.S.; supervision and project administration were carried out by A.P. and D.S.; funding acquisition was approved by A.P., D.S., L.P. and A.Me.; software was optimized by A.P.; resources were provided by V.T., L.D., A.Me., E.V., G.V., A.P., and D.S.; significant clinical suggestions for discussion–writing were given by A.Me., V.T., L.D., and G.V.

Funding This work was supported by Fondazione AIRC per la Ricerca sul Cancro IG 2017 (Grant number 20259) to DS; MFAG 2020 (Grant number 25040) to APu; IG 2019 (Grant number 23211) to LP; CAR-T Grant RCR-2019-23669115 to DS; Ricerca Locale 2022 Università degli Studi di Torino to DS; Ricerca Locale 2019 Università degli Studi di Torino to APu; Fondazione CRT 2022 to APu; Programma Operativo Nazionale (PON) 2014-2020, DM 1062/2021 PNR 2021–2027 to AMe; Italian Ministry of Health, Ricerca Corrente 2023–2024 to Candiolo Cancer Institute, FPO—IRCCS.

Data availability All data supporting this study are included in the published article and its Supplementary files. Raw datasets and source codes for image analysis will be made available from the corresponding author upon reasonable request.

Declarations

Conflict of interest The authors declare no potential conflicts of interest.

Ethical approval Peripheral blood mononuclear cells of patients with advanced stage tumors were collected at Candiolo Cancer Institute and San Luigi Hospital, after releasing written informed consent according to internal Institutional Review Board (IRB)-approved protocols (no. 225/2015; no. 125/2022), per the Declaration of Helsinki guidelines.

Consent for publication All the authors gave consent for publication.

References

1. van Baal JOAM, van Noorden CJF, Nieuwland R, Van de Vijver KK, Sturk A, van Driel WJ et al (2017) Development of peritoneal carcinomatosis in epithelial ovarian cancer: a review. J Histochem Cytochem 66(2):67–83
2. Burg L, Timmermans M, van der Aa M, Boll D, Rovers K, de Hingh I et al (2020) Incidence and predictors of peritoneal metastases of gynecological origin: a population-based study in the Netherlands. J Gynecol Oncol. https://doi.org/10.3802/jgo.2020.31.e58
3. Matulonis UA, Sood AK, Fallowfield L, Howitt BE, Sehouli J, Karlan BY (2016) Ovarian cancer. Nat Rev Dis Primers 2(1):16061
4. Breusa S, Zilio S, Catania G, Bakrin N, Kryza D, Lollo G (2023) Localized chemotherapy approaches and advanced drug delivery strategies: a step forward in the treatment of peritoneal carcinomatosis from ovarian cancer. Front Oncol. https://doi.org/10.3389/fonc.2023.1125868
5. Cortés-Guiral D, Hübner M, Alyami M, Bhatt A, Ceelen W, Glehen O et al (2021) Primary and metastatic peritoneal surface malignancies. Nat Rev Dis Primers 7(1):91
6. Ma L, Shao W, Zhu W (2024) Exploring the molecular mechanisms and potential therapeutic strategies of ferroptosis in ovarian cancer. Biocell 48(3):379–386
7. Kim SI, Kim JW (2021) Role of surgery and hyperthermic intraperitoneal chemotherapy in ovarian cancer☆. ESMO Open 6(3):100149
8. Nag S, Aggarwal S, Rauthan A, Warrier N (2022) Maintenance therapy for newly diagnosed epithelial ovarian cancer– a review. J Ovar Res 15(1):88
9. González-Martín A, Pothuri B, Vergote I, DePont CR, Graybill W, Mirza MR et al (2019) Niraparib in Patients with newly diagnosed advanced ovarian cancer. N Engl J Med 381(25):2391–2402
10. Ray-Coquard I, Pautier P, Pignata S, Pérol D, González-Martín A, Berger R et al (2019) Olaparib plus Bevacizumab as first-line maintenance in ovarian cancer. N Engl J Med 381(25):2416–2428
11. Won-Hee Y, Anna D, Lawrence K (2023) Immune checkpoint inhibitors in ovarian cancer: Where do we go from here? Cancer Drug Resist 6(2):358–377
12. Coccolini F, Gheza F, Lotti M, Virzì S, Iusco D, Ghermandi C et al (2013) Peritoneal carcinomatosis. World J Gastroenterol 19(41):6979–6994
13. de Bree E, Tsiftsis DD (2007) Principles of perioperative intraperitoneal chemotherapy for peritoneal carcinomatosis. In: González-Moreno S (ed) Advances in peritoneal surface oncology. Springer, Berlin Heidelberg, pp 39–51
14. Center ULCC, Health NIo (2021) Phase I study of autologous CAR T-cells targeting the B7-H3 antigen in recurrent epithelial ovarian. https://classic.clinicaltrials.gov/show/NCT04670068
15. Center CoHM, Institute NC (2022) Modified immune cells (TAG72-CAR T Cells) for the treatment of patients with platinum resistant epithelial ovarian cancer. https://classic.clinicaltrials.gov/show/NCT05225363
16. Pennsylvania Uo, Health NIo (2017) Tmunity therapeutics awosoKP. CAR T cells in mesothelin expressing cancers. https://classic.clinicaltrials.gov/show/NCT03054298
17. Center HLMC, Institute R (2022) Anixa Biosciences I. Infusion of autologous T cells engineered to target FSH receptor in recurrent ovarian cancer. https://classic.clinicaltrials.gov/show/NCT05316129
18. Maalej KM, Merhi M, Inchakalody VP, Mestiri S, Alam M, Maccalli C et al (2023) CAR-cell therapy in the era of solid tumor treatment: current challenges and emerging therapeutic advances. Mol Cancer 22(1):20
19. Pan K, Farrukh H, Chittepu VCSR, Xu H, Pan C-x, Zhu Z (2022) CAR race to cancer immunotherapy: from CAR T, CAR NK to CAR macrophage therapy. J Exp Clin Cancer Res 41(1):119
20. Sterner RC, Sterner RM (2021) CAR-T cell therapy: current limitations and potential strategies. Blood Cancer J 11(4):69
21. Yang B, Chen K, Liu X, Liu W, Ma Y, Tian X et al (2023) Advance in tumor immunotherapy: establishing a new paradigm for oncological treatment. Transl Surg Oncol 1(2):30–43
22. Grunewald L, Lam T, Andersch L, Klaus A, Schwiebert S, Winkler A et al (2021) A reproducible bioprinted 3D tumor model serves as a preselection tool for CAR T cell therapy optimization. Front Immunol. https://doi.org/10.3389/fimmu.2021.689697
23. Sangiolo D (2011) Cytokine induced killer cells as promising immunotherapy for solid tumors. J Cancer 2:363–368
24. Schmidt-Wolf IG, Lefterova P, Mehta BA, Fernandez LP, Huhn D, Blume KG et al (1993) Phenotypic characterization and identification of effector cells involved in tumor cell recognition of cytokine-induced killer cells. Exp Hematol 21(13):1673–1679
25. Cappuzzello E, Vigolo E, D'Accardio G, Astori G, Rosato A, Sommaggio R (2023) How can Cytokine-induced killer cells overcome CAR-T cell limits. Front Immunol. https://doi.org/10.3389/fimmu.2023.1229540
26. Rotolo R, Leuci V, Donini C, Cykowska A, Gammaitoni L, Medico G et al (2019) CAR-based strategies beyond T Lymphocytes: integrative opportunities for cancer adoptive immunotherapy. Int J Mol Sci 20(11):2839
27. Albelda SM (2020) Tumor antigen heterogeneity: the "elephant in the room" of adoptive T-cell therapy for solid tumors. Cancer Immunol Res 8(1):2
28. Leuci V, Donini C, Grignani G, Rotolo R, Mesiano G, Fiorino E et al (2020) CSPG4-specific CARCIK lymphocytes as a novel therapy for the treatment of multiple soft-tissue sarcoma histotypes. Clin Cancer Res 26(23):6321–6334
29. Magnani CF, Mezzanotte C, Cappuzzello C, Bardini M, Tettamanti S, Fazio G et al (2018) Preclinical efficacy and safety of CD19CAR cytokine-induced killer cells transfected with sleeping beauty transposon for the treatment of acute lymphoblastic leukemia. Hum Gene Ther 29(5):602–613
30. Giraudo L, Cattaneo G, Gammaitoni L, Iaia I, Donini C, Massa A et al (2023) CSPG4 CAR-redirected cytokine induced killer lymphocytes (CIK) as effective cellular immunotherapy for HLA class I defective melanoma. J Exp Clin Cancer Res 42(1):310
31. Ren X, Ma W, Lu H, Yuan L, An L, Wang X et al (2015) Modification of cytokine-induced killer cells with chimeric antigen receptors (CARs) enhances antitumor immunity to epidermal growth factor receptor (EGFR)-positive malignancies. Cancer Immunol Immunother 64(12):1517–1529
32. Zuo S, Wen Y, Panha H, Dai G, Wang L, Ren X et al (2017) Modification of cytokine-induced killer cells with folate receptor alpha (FRα)-specific chimeric antigen receptors enhances their antitumor immunity toward FRα-positive ovarian cancers. Mol Immunol 85:293–304
33. Merker M, Wagner J, Kreyenberg H, Heim C, Moser LM, Wels WS et al (2020) ERBB2-CAR-engineered cytokine-induced killer cells exhibit both CAR-mediated and innate immunity against high-risk Rhabdomyosarcoma. Front Immunol. https://doi.org/10.3389/fimmu.2020.581468
34. Chang K, Pastan I (1996) Molecular cloning of mesothelin, a differentiation antigen present on mesothelium, mesotheliomas, and ovarian cancers. Proc Natl Acad Sci 93(1):136–140

35. Morello A, Sadelain M, Adusumilli PS (2016) Mesothelin-targeted CARs: driving T cells to solid tumors. Cancer Discov 6(2):133–146
36. Coelho R, Ricardo S, Amaral AL, Huang Y-L, Nunes M, Neves JP et al (2020) Regulation of invasion and peritoneal dissemination of ovarian cancer by mesothelin manipulation. Oncogenesis 9(6):61
37. Weidemann S, Gorbokon N, Lennartz M, Hube-Magg C, Fraune C, Bernreuther C et al (2023) High homogeneity of mesothelin expression in primary and metastatic ovarian cancer. Appl Immunohistochem Mol Morphol. https://doi.org/10.1097/PAI.0000000000001097
38. Medico E, Russo M, Picco G, Cancelliere C, Valtorta E, Corti G et al (2015) The molecular landscape of colorectal cancer cell lines unveils clinically actionable kinase targets. Nat Commun 6(1):7002
39. Amendola M, Venneri MA, Biffi A, Vigna E, Naldini L (2005) Coordinate dual-gene transgenesis by lentiviral vectors carrying synthetic bidirectional promoters. Nat Biotechnol 23(1):108–116
40. Naber HPH, Wiercinska E, Ten Dijke P, Van Laar T (2011) Van Laar T (2011) Spheroid Assay to Measure TGF-β-induced Invasion. JoVE 57:e3337
41. Galeano Niño JL, Pageon SV, Tay SS, Colakoglu F, Kempe D, Hywood J et al (2020) Cytotoxic T cells swarm by homotypic chemokine signalling. Elife 9:e56554
42. Ronteix G, Jain S, Angely C, Cazaux M, Khazen R, Bousso P et al (2022) High resolution microfluidic assay and probabilistic modeling reveal cooperation between T cells in tumor killing. Nat Commun 13(1):3111
43. Katz SC, Point GR, Cunetta M, Thorn M, Guha P, Espat NJ et al (2016) Regional CAR-T cell infusions for peritoneal carcinomatosis are superior to systemic delivery. Cancer Gene Ther 23(5):142–148
44. Xia Ang W, Li Z, Chi Z, Du S-H, Chen C, Tay JCK et al (2017) Intraperitoneal immunotherapy with T cells stably and transiently expressing anti-EpCAM CAR in xenograft models of peritoneal carcinomatosis. Oncotarget 8(8):13545
45. Adusumilli PS, Zauderer MG, Rivière I, Solomon SB, Rusch VW, O'Cearbhaill RE et al (2021) A phase I trial of regional mesothelin-targeted CAR T-cell therapy in patients with malignant pleural disease, in combination with the Anti–PD-1 agent Pembrolizumab. Cancer Discov 11(11):2748–2763
46. Katz SC, Burga RA, McCormack E, Wang LJ, Mooring W, Point GR et al (2015) Phase I hepatic immunotherapy for metastases study of intra-arterial chimeric antigen receptor-modified T-cell therapy for CEA+ liver metastases. Clin Cancer Res 21(14):3149–3159
47. Guo Y, Tong C, Wu Z, Lu Y, Wang Y, Han W (2023) Reciprocal activation of antigen-presenting cells and CAR T cells triggers a widespread endogenous anti-tumor immune response through sustained high-level IFNγ production. Cancer Biol Med. https://doi.org/10.20892/j.issn.2095-3941.2023.0324
48. Wang X, Qiu W, Liu H, He M, He W, Li Z et al (2023) The inducible secreting TLR5 agonist, CBLB502, enhances the anti-tumor activity of CAR133-NK92 cells in colorectal cancer. Cancer Biol Med 12(365):265
49. DeSelm C, Palomba ML, Yahalom J, Hamieh M, Eyquem J, Rajasekhar VK et al (2018) Low-dose radiation conditioning enables CAR T cells to mitigate antigen escape. Mol Ther 26(11):2542–2552
50. Upadhyay R, Boiarsky JA, Pantsulaia G, Svensson-Arvelund J, Lin MJ, Wroblewska A et al (2021) A critical role for fas-mediated off-target tumor killing in T-cell immunotherapy. Cancer Discov 11(3):599–613
51. Esther S, Thomas P, Ibrahim E-S, Ying Z, Rui H, Alina M et al (2023) Tuned activation of MSLN-CAR T cells induces superior antitumor responses in ovarian cancer models. J Immunother Cancer 11(2):e005691
52. Lanitis E, Poussin M, Hagemann IS, Coukos G, Sandaltzopoulos R, Scholler N et al (2012) Redirected antitumor activity of primary human lymphocytes transduced with a fully human anti-mesothelin chimeric receptor. Mol Ther 20(3):633–643
53. Kim S, Kim B, Song YS (2016) Ascites modulates cancer cell behavior, contributing to tumor heterogeneity in ovarian cancer. Cancer Sci 107(9):1173–1178
54. Hrvat A, Schmidt M, Wagner B, Zwanziger D, Kimmig R, Volbracht L et al (2023) Electrolyte imbalance causes suppression of NK and T cell effector function in malignant ascites. J Exp Clin Cancer Res 42(1):235
55. Chen C, Leng X, Zhang YU, Hu J, Wei D, Wang P et al (2023) Effects of platelets on characteristics of lymphocytes cultured in vitro and optimization of adoptive immunotherapy. Biocell 47(12):2661–2669
56. Ranoa DRE, Sharma P, Schane CP, Lewis AN, Valdez E, Marada VVVR et al (2023) Single CAR-T cell treatment controls disseminated ovarian cancer in a syngeneic mouse model. J Immunother Cancer 11(5):e006509